J. Fluid Mech. (2012), *vol.* 698, *pp.* 446–467.
doi:10.1017/jfm.2012.119

Boundary-element method for the prediction of performance of flapping foils with leading-edge separation

Yulin Pan, Xiaoxia Dong, Qiang Zhu‡ and Dick K. P. Yue†

Department of Mechanical Engineering, Massachusetts Institute of Technology, Cambridge, MA 02139, USA

(Received 22 August 2011; revised 21 February 2012; accepted 27 February 2012; first published online 12 April 2012)

A numerical model based on a boundary-element method is developed to predict the performance of flapping foils for the general cases where vorticities are shed near the leading edge as well as from the trailing edge. The shed vorticities are modelled as desingularized thin shear layers which propagate with the local flow velocity. Special treatments are developed to model the unsteady and alternating leading-edge separation (LES), which is a main element of difficulty for theoretical and numerical analyses of general flapping foils. The present method is compared with existing experiments where it is shown that the inclusion of LES significantly improves the prediction of thrust and efficiency, obtaining excellent agreement with measurements over a broad range of flapping frequencies (Strouhal number) and motion amplitudes (maximum angle of attack). It is found that the neglect of LES leads to substantial over-prediction of the thrust (and efficiency). The effects of LES on thrust generation in terms of the circulation around the foil, the steady and unsteady thrust components, and the vortex-induced pressure on the foil are elucidated. The efficiency and robustness of the method render it suitable for design optimization which generally requires large numbers of performance evaluations. To illustrate this, we present a sample problem of designing the flapping motion, with the inclusion of higher harmonic components, to maximize the efficiency under specified thrust. When optimal higher harmonic motions are included, the performance of the flapping foil is appreciably improved, mitigating the adverse effects of LES vortex on the performance.

Key words: flow–structure interactions, propulsion

1. Introduction

The superior swimming performance of many aquatic creatures employing flapping (large-amplitude heaving and pitching) fins and appendages have attracted theoretical, experimental and numerical investigations of the performance of flapping foils (e.g. Theodorsen 1935; Anderson *et al.* 1998; Lewin & Haj-Hariri 2003; Read, Hover & Triantafyllou 2003) and their potential marine applications (e.g. Licht, Hover & Triantafyllou 2004).

† Email address for correspondence: yue@mit.edu

‡ Present address: Department of Structural Engineering, University of California, San Diego, La Jolla, CA 92093, USA.

Much of the activity is experimental work, involving quantitative measurements of the motion dynamics and flow visualization.

Recent measurements by Anderson *et al.* (1998) and Read *et al.* (2003) show that, with properly selected motion parameters, flapping foils can achieve high efficiencies even under large loadings, making it attractive relative to propellers. For example, efficiency as high as 87 % (close to the theoretically achievable actuator disk value) for a thrust coefficient of around 0.67 has been reported (Anderson *et al.* 1998). In contrast, small high-loading propellers used in underwater vehicles are usually typically no more than 40 % efficient (Triantafyllou & Triantafyllou 1995). Owing to the large motion amplitudes involved, almost all of these high thrust production cases involve substantial leading-edge separation (LES). The specific role of the LES is however not elucidated.

Flow visualization around the foil offers useful but limited insight. Koochesfahani (1989) observed the wake behind a pitching foil and showed that two vorticities of the same sign are shed in each half-cycle of the oscillation, consistent with the presence of LES, even for relatively small pitching motion ($\sim 4^\circ$ amplitude). For a flapping foil, Anderson *et al.* (1998) showed that leading-edge (LE) vortices are formed when the maximum angle of attack during the motion, α_{max}, exceeds a threshold value. While the precise value of this threshold depends on the Strouhal number (S_t) and the heaving amplitude-to-chord ratio (h_0/c), it is clear that LES plays an important role in flapping foil dynamics for all but very small motion amplitudes.

The lack of understanding of LES hampers theoretical and numerical investigations of the flapping foil especially in the context of potential flow. In the absence of LES, the classical theoretical solution is given by Theodorsen (1935) (and by Kármán & Sears 1938) who solve the linearized potential flow around a flat plate undergoing small oscillating motion. Streitlien & Triantafyllou (1995) extend this to arbitrary unsteady motions, using conformal mapping, with point vortices shedding from the trailing edge (TE) convected with the local flow. Within the same framework, solutions for general geometries and motions are available numerically using a boundary-element method (BEM) (e.g. Katz & Plotkin 1991; Zhu *et al.* 2002).

There are early successful attempts to include LES in the potential flow solution of the foil problem. Many of these are for a plate wherein the LES point is naturally fixed at the plate edge and is therefore prescribed. These include Sarpkaya (1975), Kiya & Arie (1977) and Katz (1981) who consider the problem of unsteady flow past stationary flat or cambered plates, modelling the shed LE/TE vorticity as discrete vortices. With the separation points prescribed, reasonable flow patterns are obtained, but the forces and strengths of the shedding vortices are generally substantially over predicted compared with experiments. The solution to this problem is appreciably improved by Jones (2003), Jones & Shelley (2005) and Shukla & Eldredge (2007) by addressing the ill-posedness associated with discrete vorticity using the desingularization scheme of Krasny (1987).

When the potential flow is coupled with a boundary-layer solution on the foil, the LES can be predicted using empirical criterion (e.g. Stratford 1959). The original formulation for such an approach was developed for the stationary foil with a finite-curvature LE (e.g. Burns 1988; Robinson 1988), and a similar methodology has been adopted to commercial applications for general 3D unsteady problems, for example, *USAERO* (see e.g. Maskew 1993).

The solution of the LES problem and the need for empirical formula(e), are, in principle, avoided in the context of full Navier–Stokes solution of the problem; and there are many recent examples of these applied to flapping foils (e.g. Lewin &

Haj-Hariri 2003; Wang 2000; Zhu & Peng 2009). The computational cost and efficacy of these results for high Reynolds number remain of concern, and these methods are still not as widely adopted for practical applications as could be expected in the future.

The present paper addresses the potential flow solution of the problem of flow past an arbitrary foil undergoing general flapping motion for which LES cannot be neglected. The physical problem involves LES from a LES point which is in general unknown, moving, and alternates between the upper and lower foil surfaces (depending on the phase of the flapping motion). Motivated by earlier computational work for modelling separated flow as shear layers, and the experimental visualization of Taneda (1977) which shows that the unsteady vorticity shedding come from a localized region on the body, we propose a potential-flow BEM solution for the finite thickness flapping foil with vorticity shedding from leading and trailing edges represented by thin (desingularized) vortex sheets. The position of LES as a function of time is not *a priori* known and a procedure is developed to obtain this as well as the strength of the shed vorticity. The approach is general and robust, and does not contain free parameters (or input from experiments) other than those associated with the desingularization/fencing of the vortex sheets. The problem is cast in 2D, although the methodology can be extended to 3D in a straightforward way.

One of the key objectives of this work is to establish the validity of the BEM solution in direct quantitative comparisons to experiments. To achieve this, we test the present method against the extensive measurements from Read *et al.* (2003) of the thrust and efficiency over a broad range of motion and frequency parameters. The comparisons are remarkably good, and significantly improve upon those obtained without LES. This lends support to the validity of the present approach, despite the simplifying assumptions inherent in the method. Comparing the BEM predictions with and without LES, it is seen that LES corrects the general over-prediction of thrust and efficiency by BEM without LES. We are able to identify the root mechanism in terms of the reduction of circulation around the foil caused by LES, and the LES vortex-induced pressure reduction on the pressure side of the foil.

The efficiency and accuracy of the method for predicting motion dynamics make it useful for design optimization of flapping foil performance to obtain desired motion parameters (or foil geometry), where large numbers of simulation evaluations may be required. We illustrate this in a design application where we find optimal values of third-harmonic motion components that can be introduced to appreciably improve the thrust (and efficiency) of the foil.

2. Problem definition

We consider a two-dimensional (2D) foil, with chord length c, undergoing prescribed harmonic heaving-pitching motion in a uniform inflow U (see figure 1 for the coordinate system and definitions). The heave motion $h(t)$ and pitch motion $\theta(t)$, about a point O distance b from the LE, are expressed as

$$h(t) = h_0 \sin(\omega t), \quad \theta(t) = \theta_0 \sin(\omega t + \psi), \tag{2.1}$$

where h_0, θ_0 are respectively the heave and pitch amplitudes, and ψ the phase lead of pitch motion relative to the heave motion. An important parameter in this study is the Strouhal number based on the heave amplitude:

$$S_t = \frac{h_0 \omega}{\pi U}. \tag{2.2}$$

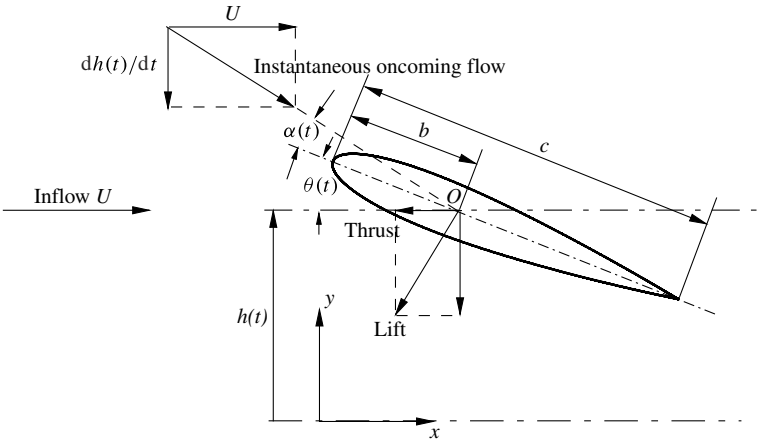

FIGURE 1. Geometry and kinematics of a flapping foil.

The instantaneous angle of attack $\alpha(t)$ due to (2.1) has contributions from both heaving and pitching motions:

$$\alpha(t) = \alpha^h(t) + \theta(t). \tag{2.3}$$

where $\alpha^h(t) = -\tan^{-1}(\dot{h}(t)/U)$ is the effective angle of attack due to heave (only).

The foil is subject to oscillatory x and y direction forces $F_x(t)$ and $F_y(t)$, torque $Q(t)$ about point O, and input power $P_{in}(t)$:

$$P_{in}(t) = -F_y(t)\dot{h}(t) - Q(t)\dot{\theta}(t). \tag{2.4}$$

For periodic motion of period $\tau = 2\pi/\omega$, we define time-averaged quantities:

$$\bar{f} \equiv \frac{1}{\tau}\int_{t_0}^{t_0+\tau} f(t)\,\mathrm{d}t, \tag{2.5}$$

and coefficients of thrust, C_T, and power, C_P:

$$C_T = \frac{T}{\frac{1}{2}\rho U^2 c}, \quad C_P = \frac{\overline{P_{in}}}{\frac{1}{2}\rho U^3 c}, \tag{2.6}$$

where $T = -\overline{F_x}$ and ρ is the fluid density. Finally, the propulsive (or Froude) efficiency η is defined as the ratio of useful power over input power,

$$\eta = \frac{TU}{\overline{P_{in}}} = \frac{C_T}{C_P}. \tag{2.7}$$

For effective thrust generation, the phase between heave $h(t)$ and pitch $\theta(t)$ is generally $\psi \approx 90^\circ$ (e.g. Isogai, Shinmoto & Watanabe 1999; Read *et al.* 2003), so that θ and α^h are approximately 180° out of phase for both the upward and downward strokes, and the problem is symmetric with respect to thrust between the upward/downward strokes. In these cases, it is convenient for later reference to define

average quantities for each stroke:

$$\bar{f}^{u,d} \equiv \frac{2}{\tau}\int_{t_{u,d}}^{t_{u,d}+\tau/2} f(t)\,\mathrm{d}t, \tag{2.8}$$

where $t_{u,d}$ is the beginning of the upward, downward stroke, respectively.

It is known from experiments (e.g. Anderson *et al.* 1998) that, in addition to S_t, the most important motion parameter governing the flapping dynamics is the maximum angle of attack in an oscillation period, α_{max},

$$\alpha_{max} \equiv \max_t |\alpha(t)| = \max_t |\alpha^h(t) + \theta(t)|. \tag{2.9}$$

Thus it is often useful to specify α_{max} and solve for θ_0 (given S_t), generally numerically (see e.g. Read *et al.* 2003), rather than the (more natural) other way around. For $\psi = 90°$, sufficiently small S_t and $\alpha_{max} < \alpha^h_{max} \equiv \max|\alpha^h(t)| = \tan^{-1}(S_t\pi)$, equation (2.9) has two solutions for θ_0, one associated with drag generation and the other with thrust production (Read *et al.* 2003). At relatively low S_t, the double solution corresponds to $\theta_0 = \alpha^h_{max} \pm \alpha_{max}$, i.e. $\alpha(t)$ having the opposite/same sign as $\alpha^h(t)$. Our interest is in the case of thrust production (plotted in figure 1), with α and α_h having the same sign when α_{max} obtains. In summary, the complete foil motion is described by S_t, α_{max}, h_0/c, ψ and b/c.

3. Solution formulation

We develop a BEM for this 2D unsteady flapping foil problem with LES, where both LE and TE shed vorticities are modelled as desingularized thin vortex sheets.

3.1. *Boundary-value problem*

In the context of potential flow, we express the total velocity $v(\boldsymbol{x}, t)$ in term of the perturbation potential $\phi(\boldsymbol{x}, t)$:

$$\boldsymbol{v}(\boldsymbol{x}, t) = \boldsymbol{U}_\infty + \nabla\phi(\boldsymbol{x}, t), \tag{3.1}$$

where $\boldsymbol{U}_\infty = (U, 0)$. With (3.1), the hydrodynamic pressure p (with zero reference pressure) is given by a Bernoulli equation

$$p(x, y, t) = -\rho\frac{\partial\phi(x, y, t)}{\partial t} - \frac{1}{2}\rho(|\nabla\phi(x, y, t)|^2 + 2U\phi_{,x}). \tag{3.2}$$

In the fluid volume $\mathscr{V}$,

$$\nabla^2\phi(\boldsymbol{x}, t) = 0. \tag{3.3}$$

On the instantaneous foil surface $\mathscr{B}(t)$, we impose the kinematic condition

$$\frac{\partial\phi(\boldsymbol{x}, t)}{\partial n} = -\boldsymbol{U}_\infty \cdot \hat{n} + \boldsymbol{u}_{foil}(\boldsymbol{x}, t) \cdot \hat{n}, \tag{3.4}$$

where $\boldsymbol{u}_{foil}(\boldsymbol{x}, t)$ is the velocity of a point on $\mathscr{B}(t)$, determined by foil motion and geometry.

We consider the general case where in addition to an evolving vortex sheet $\mathscr{T}(t)$ (with potential jump $\Delta\phi_{\mathscr{T}}(\boldsymbol{x}, t)$) shed from the TE, an evolving LE vortex sheet $\mathscr{L}(t)$ (with potential jump $\Delta\phi_{\mathscr{L}}(\boldsymbol{x}, t)$) is shed from some (time-varying) LES point $X_{LE}(t)$ (yet to be determined). Let $\Delta\phi^0_{\mathscr{T}}$ and $\Delta\phi^0_{\mathscr{L}}$ be the potential jump across $\mathscr{T}(t)$ and $\mathscr{L}(t)$ at TE and the LES point $X_{LE}(t)$, respectively. At the TE, $\Delta\phi^0_{\mathscr{T}}$ can be

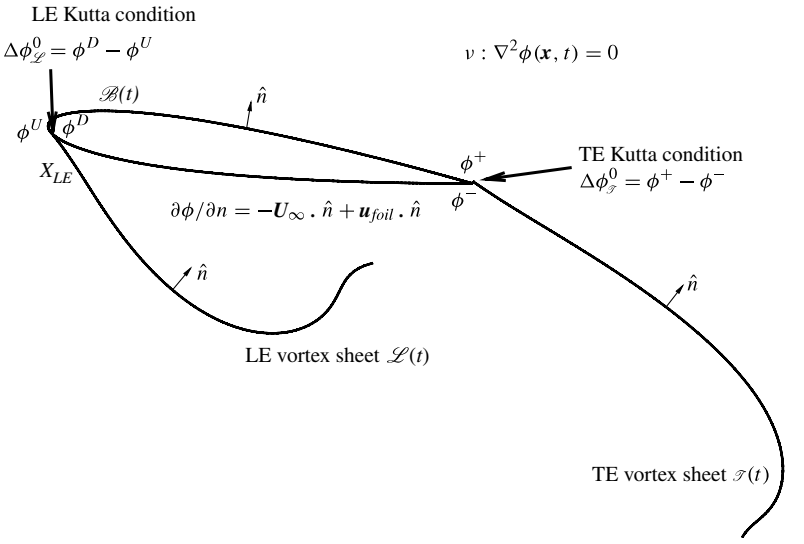

FIGURE 2. Boundary-value problem for a flapping foil with LE and TE shed vortex sheets.

determined from the Kutta condition (of finite velocity). Ignoring unsteady effects, this can be obtained by, say, a Morino condition (Morino & Kuo 1974):

$$\Delta\phi^0_{\mathscr{T}} = \phi^+ - \phi^-, \tag{3.5}$$

where ϕ^+ and ϕ^- are the values of ϕ on upper and lower TE; and the condition ensures continuation of the quasi-steady pressure at the TE. The more precise Kutta condition for the unsteady problem requires vanishing pressure jump across the TE (e.g. Kinnas & Hsin 1992). The difference between this and (3.5) is found to be small in predicting global averaged results (such as thrust and efficiency) (e.g. Hess 1990), for all but very large $S_t(\gtrsim O(1))$. For the latter, experimental evidence indicates that the pressure loading at TE may in fact be non-zero (e.g. Satyanarayana & Davis 1978; McCroskey 1982).

For the LES, we apply a similar Morino condition:

$$\Delta\phi^0_{\mathscr{L}} = \phi^D - \phi^U, \tag{3.6}$$

where ϕ^U and ϕ^D are the values of ϕ upstream and downstream of $X_{LE}(t)$, respectively. At the LE, equation (3.6) ensures the continuity of the (quasi-steady) pressure across X_{LE}. Similar Kutta conditions have been applied successfully at a separation point located on a finite-curvature boundary (see, e.g. Katz 1981).

The boundary-value problem above (figure 2) is solved using the BEM. At any point $\mathscr{P}$ on $\mathscr{B}(t)$, we have

$$\frac{\phi(\mathscr{P}, t)}{2} = \int_{\mathscr{B}(t)} \left[-\phi(q, t)\frac{\partial G(\mathscr{P}; q)}{\partial n_q} + G(\mathscr{P}; q)\frac{\partial \phi(q, t)}{\partial n_q} \right] \mathrm{d}\ell_q$$
$$- \int_{\mathscr{T}(t)} \Delta\phi_{\mathscr{T}}(q, t)\frac{\partial G(\mathscr{P}; q)}{\partial n_q}\,\mathrm{d}s_q - \int_{\mathscr{L}(t)} \Delta\phi_{\mathscr{L}}(q, t)\frac{\partial G(\mathscr{P}; q)}{\partial n_q}\,\mathrm{d}s_q, \tag{3.7}$$

where $G(\mathscr{P}; q) = \ln|\boldsymbol{R}(\mathscr{P}; q)|/(2\pi)$ is the 2D Green function, $\boldsymbol{R} \equiv \mathscr{P} - q$, $\hat{n}$ is the unit vector normal to the integration surface; and, for clarity, ℓ, s respectively the

arclengths along $\mathscr{B}$ and $\mathscr{T}$, $\mathscr{L}$. Equation (3.7) expresses the potential $\phi(\boldsymbol{x}, t)$ on the foil surface as a combination induced by a source distribution $\partial\phi/\partial n$ on $\mathscr{B}(t)$, and dipole distributions ϕ, $\Delta\phi_{\mathscr{T}}$ and $\Delta\phi_{\mathscr{L}}$ on $\mathscr{B}(t)$, $\mathscr{T}(t)$ and $\mathscr{L}(t)$. Among these variables, $\partial\phi/\partial n$ on $\mathscr{B}(t)$ is prescribed by (3.4); $\Delta\phi_{\mathscr{T}}$ and $\Delta\phi_{\mathscr{L}}$ are known from previous time, except the newly shedding dipole strength $\Delta\phi^0_{\mathscr{T}}$ and $\Delta\phi^0_{\mathscr{L}}$ which are given by (3.5) and (3.6) (in terms of ϕ on $\mathscr{B}(t)$). At a given time t, the boundary-value problem ((3.7) with (3.4)–(3.6)) is solved for the (only) unknown ϕ on $\mathscr{B}(t)$.

3.2. *Treatment of TE and LE vortex sheets*

The choice of a single separation point $X_{LE}(t)$ to model LES is suggested by observations of highly localized separation for flapping foils and related problems (e.g. Taneda 1977; Degani, Li & Walker 1996). The precise location of $X_{LE}(t)$ (at any time) near the LE region is however unknown. In the present work, we use a heuristic criterion to determine $X_{LE}(t)$, arguing physically that $X_{LE}(t)$ should be near the LE pressure suction peak, given by

$$\left.\frac{\partial p}{\partial \ell}\right|_{X_{LE}(t)} = 0, \qquad \left.\frac{\partial^2 p}{\partial \ell^2}\right|_{X_{LE}(t)} > 0. \tag{3.8}$$

The choice of (3.8) can be motivated in terms of the vorticity flux ($\omega_n \equiv \boldsymbol{\nabla}\omega \cdot \hat{n}$) near the LE when LES occurs, which provides the vorticity ejected into the flow. Evaluating the momentum equation along the body surface, ω_n is directly related to the wall pressure gradient, $\omega_n \sim \partial p/\partial \ell$ (e.g. Reynolds & Carr 1985). For general flapping foils, it has been observed (e.g. Visbal 1991; Acharya & Metwally 1992) that ω_n is concentrated in two small regions upstream and downstream of and very close to the pressure suction peak. The use of a single LES and (3.8) represents a simple approximation of the above physical picture wherein X_{LE} is placed at the intermediate maximum suction pressure point. The ultimate validity of the LES model and in particular (3.8) for predicting the performance of flapping foils must be subsequently supported by comparison with measurements, which is the main objective of this work.

In general, $X_{LE}(t)$ determined by (3.8) is not fixed in time, and our method captures this by solving the pressure profile on $\mathscr{B}(t)$ at each time step and updating $X_{LE}(t)$ according to (3.8). During the shedding, the LES at each time step is solved with a newly determined X_{LE} (and existing vortex sheets) in conjunction with the condition (3.6) which provides the jump in ϕ at X_{LE}. For flapping motions with limited α_{max}, the movement of the minimum pressure point along the upper/lower surface turns out to be relatively small, and not much influenced by the addition of a new vortex sheet. This is known from experiments (e.g. Acharya & Metwally 1992) and also confirmed in our simulations. It is then possible to assume a fixed position for X_{LE}, which can be determined from, say, the time of initial separation for a $\mathscr{L}(t)$. Subsequently, the numerical procedure is considerably simplified, without an appreciable impact on the results.

For flapping motion, the numerical solution requires switching of the LES between the upper and lower foil surfaces during an oscillation cycle, depending on the phase of the motion. To implement this, we apply a switching criterion wherein, at a given instant, LES is specified to be from that foil surface whose shedding tendency is greater. At every time step, we apply (3.6) on respectively only X_{LE} on upper or lower surface, and determine the side where LES occurs to be that for which the potential jump $|\Delta\phi^0_{\mathscr{L}}|$ is greater. Since $|\Delta\phi^0_{\mathscr{L}}|$ for a given $\mathscr{L}(t)$ always increases from zero

when the new vortex sheet is initiated, the switch occurs only when intensities of both the old and new shedding are small. Thus, there is effectively no jump in the solution ϕ on $\mathscr{B}$ during a switch. For the harmonic flapping motions we consider in § 5, the switching typically occurs twice per oscillation cycle, as expected, consistent with experimental visualization (see e.g. figures 7 and 8). After N cycles, $2N$ LE vortex sheets are shed into the flow field.

The LE and TE vortex sheets $\mathscr{L}(t)$ and $\mathscr{T}(t)$ (and associated dipole strengths $\Delta\phi$) are advected by the local flow velocity over time. To avoid the singularity associated with the induced velocity of a thin vortex sheet, we apply the desingularization method of Krasny (1987). The desingularized local velocity at a point $\mathscr{P}$ on $\mathscr{L}(t)$ or $\mathscr{T}(t)$ is expressed as

$$\boldsymbol{u}_{\delta_s}(\mathscr{P}, t) = \boldsymbol{U}_\infty + \boldsymbol{u}_{\mathscr{B}}(\mathscr{P}, t) + \frac{1}{2\pi}\int_{\mathscr{L}(t),\mathscr{T}(t)} \left[\frac{\partial\Delta\phi(q,t)}{\partial s}\frac{\hat{k}\times\boldsymbol{R}(\mathscr{P};q)}{|\boldsymbol{R}(\mathscr{P};q)|^2+\delta_s^2}\right] \mathrm{d}s_q, \quad (3.9)$$

where $0 < \delta_s \ll 1$ is a desingularization parameter. In (3.9), $\boldsymbol{u}_{\mathscr{B}}(\mathscr{P}, t)$ represents the induced velocity due to the source and dipole distribution along the body $\mathscr{B}(t)$ (cf. (3.7)) and can be evaluated by standard method (see e.g. Katz & Plotkin 1991).

An issue encountered in the propagation of $\mathscr{L}(t)$ is the vortex sheet–body interaction problem. Depending on the foil geometry and motion (and computational parameters), it is possible for $\mathscr{L}(t)$ to approach (and possibly cross) $\mathscr{B}(t)$ in the simulation. For the periodic flapping problem we consider, this mainly occurs in two situations: (i) $\mathscr{L}(t)$ approaches $\mathscr{B}(t)$ from outside due to motions of either or both of them; (ii) when $\alpha(t)$ is small enough, the newly shed vortex moves onto (instead of away from) $\mathscr{B}(t)$ (e.g. Jones 2003; Jones & Shelley 2005). In the present numerical approach, the penetration of $\mathscr{L}(t)$ into $\mathscr{B}(t)$ is circumvented/prevented by introducing two schemes: (*a*) we apply the desingularization (δ_s) also in the evolutions of $\boldsymbol{u}_{\mathscr{B}}(p, t)$; and (*b*) we introduce a 'fencing' scheme associated with small parameter ϵ_b, so that whenever a vortex comes within a distance ϵ_b of $\mathscr{B}(t)$, it is relocated and placed on the nearest point on the fence (repulsive advection, e.g. Peace & Riley 1983, is not modelled in the present approach). Provided that the normal advection velocity of the vortex relative to the foil remains non-positive, $\mathscr{L}(t)$ will tend to remain (re)attached to $\mathscr{B}(t)$ ($+\epsilon_b$) (see e.g. the lower surface of $\mathscr{B}(t)$ in figure 7(*a*),(*b*) for scenarios (ii) and (i) above, respectively). When the relative normal advection velocity becomes positive, it is possible for $\mathscr{L}(t)$ to be detached (again) from $\mathscr{B}(t)$. Similar fencing treatment has been used successfully, for example, in propeller vortex–blade interaction problems (e.g. Yao & Liu 1998; He 2010).

For numerical implementation of the BEM solution, we discretize (3.7) and (3.9) using constant panel method (piecewise linear geometry and constant singularity strengths, e.g. Katz & Plotkin 1991). For $\mathscr{B}$, we use N_ℓ cosine-spaced panels; while for $\mathscr{T}$, $\mathscr{L}$, the segment size (distance between the vortex blobs) are determined by the time step (and local velocity).

The overall initial-boundary-value problem (starting from quiescent initial state) is solved as follows. (*a*) At any instant time, t, we check if a switch of X_{LE} occurs by the switching criterion. The position of X_{LE} is updated according to (3.8) if switch occurs, but otherwise fixed. (*b*) (3.7) with (3.4)–(3.6) is used to determine $\phi(\boldsymbol{x}, t)$ on $\mathscr{B}$, as well as the newly-shedding dipole strengths $\Delta\phi^0_{\mathscr{T}}(t)$ and $\Delta\phi^0_{\mathscr{L}}(t)$. (*c*) The vortex sheet positions $\mathscr{T}$, $\mathscr{L}$ (as well as $\Delta\phi_{\mathscr{T}}$ and $\Delta\phi_{\mathscr{L}}$) are advected forward in time according to (3.9) via an explicit Euler scheme, and $\mathscr{B}$ is updated according to the prescribed

motion. The procedure (*a*)–(*c*) is repeated at $t = t + \Delta t$ until limit cycle is reached, and the relevant quantities (2.6), (2.7) evaluated.

We remark that the numerical method above, especially (3.8), is somewhat specific to problems such as flapping foils, for which LES is confined in a relatively small region near the LE. While it might be tempting to extend this inviscid BEM approach to more general geometries (say a circular cylinder, see e.g. Sarpkaya & Shoaff 1979), additional issues associated with, for example, the motion of the unsteady separation points (e.g. Haller 2004), the synchronicity between/among the vortex shedding at different points, and the effective modelling of the complex wake with discrete vortex sheets, must be addressed. Indeed, the objective of the present work is to show that the relative simple approach we describe (with the simplifying assumptions and modelling) can be effective for the specific problem of predicting the performance characteristics of foil-like geometries in flapping motion. This is the purpose of § 5.

4. Numerical convergence

The key computational parameters of the present method (LES BEM) are δ_s, ϵ_b, N_ℓ and Δt. For given N_ℓ and Δt (which determine average body panel size $\Delta\ell_0$ and average vortex sheet segment length Δs_0), the numerical method converges for desingularization/fencing parameters δ_s, ϵ_b greater than some minimum threshold values $\delta_{s,min}$, $\epsilon_{b,min}$. Figure 3(*a*) shows that the predictions on the two performance quantities of interest, C_T and η, are relatively insensitive to the values of $\delta_s > \delta_{s,min}$. For numerics, we fix $\delta_{s,min}$ as the value above which the performance predictions change by less than some specified tolerance. The specific value of $\delta_{s,min}$ is found to depend on the physical flapping parameters, in particular the maximum angle of attack α_{max}. The dependence $\delta_{s,min}(\alpha_{max})$ is closely linear (see figure 4), which provides a simple fit for the choice of the desingularization parameter. Note that the actual value of $\delta_s (= O(0.1 \sim 0.3)$ from figure 4) depends on the specifics of the numerics (and not on actual real fluid effects), and is not as small as might be expected based on the latter considerations.

Similar behaviours also hold for ϵ_b (shown in figure 3*b*). In general, $\epsilon_{b,min}$ is not sensitive to the motion parameters, and therefore is chosen to be $0.02c$ for all of the cases, which provides stable numerical results.

Fixing δ_s, ϵ_b ($> \delta_{s,min}, \epsilon_{b,min}$), the numerical method converges approximately linearly with body panel size $\Delta\ell_0$ for smooth foils (e.g. Bellamy-Knights *et al.* 1989). The convergence with time step Δt (which also controls Δs_0) is limited from above by the instability of the Euler integration, and from below by the instability of the vortex sheets, as discussed in Krasny (1987). This is shown in figure 3(*b*).

Based on extensive convergence/sensitivity tests similar to the above, in all subsequent results, we use $N_\ell = 250$, $\Delta t/(c/U) = 0.01$, $\delta_s = \delta_{s,min} \approx (0.005\alpha_{max} + 0.09)c$, and $\epsilon_b = \epsilon_{b,min} \approx 0.02c$. In our simulations (of harmonic flapping starting from rest), limit cycle of the performance metrics are typically reached after 1∼2 periods (independent of the initial motion phase), and averaged coefficients such as (2.6) are obtained with $t_0 \gtrsim 2\tau$. With these choices of numerical parameters, all of the predictions of C_T and η are convergent to less than $O(5\,\%)$.

The typical computational time for each case is $O(5)$ minutes, running on a PC with a single-core Intel Pentium CPU (3.4 GHz). The addition of LES increases the overall computational effort by ∼50 %, compared with that with just the TE vortex sheet. These computational efforts are several orders of magnitude smaller than typical Navier–Stokes simulations of such problems.

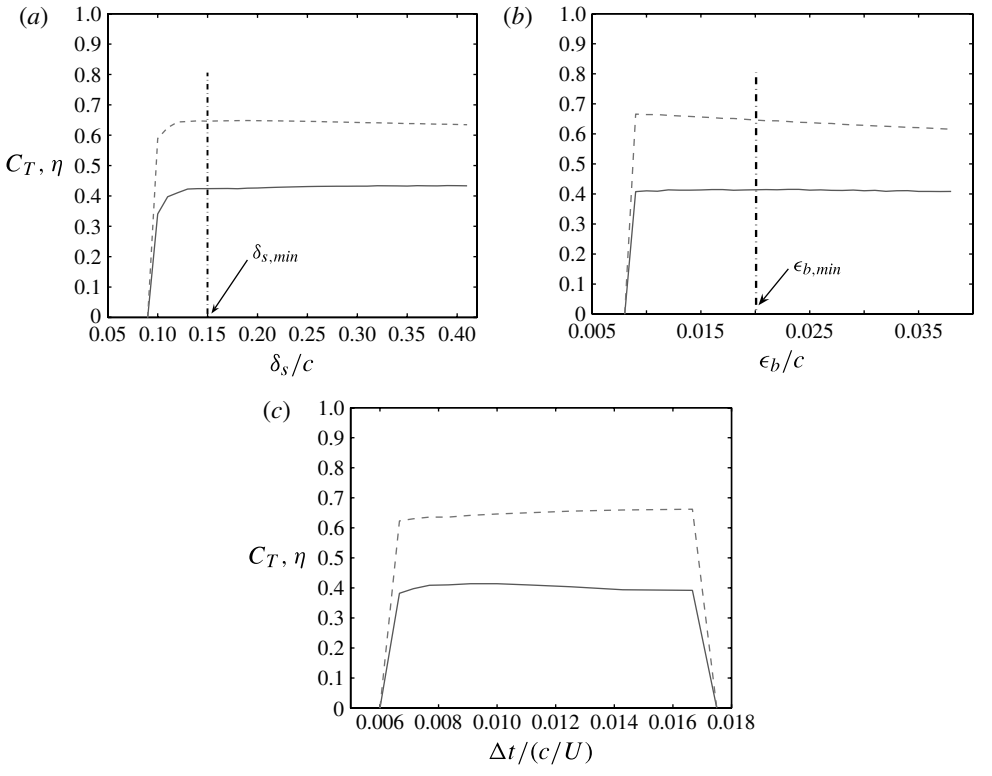

FIGURE 3. LES BEM predictions of C_T (—) and η (– – –) with varying: (*a*) desingularization parameter δ_s/c (the value of the desingularization parameter used in the simulations, $\delta_{s,min}$, is identified); (*b*) fencing parameter ϵ_b/c (the value of the fencing parameter used in the simulations, $\epsilon_{b,min}$, is identified); and (*c*) time step $\Delta t/(c/U)$. The motion parameters are $h_0/c = 1.0$, $S_t = 0.3$, $\alpha_{max} = 15°$.

5. Numerical results

Our main objective is to show that the present LES BEM method obtains (sufficiently improved) predictions of flapping performance that compares well with experiments. Motivated by the extensive measurements of Read *et al.* (2003), we use their foil and flapping geometry (NACA0012 foil and $b/c = 1/3$). In the experiments, the foil has relatively high aspect ratio ($span = 6c$), fitted with endplates, which justifies the use of our 2D model. Before we show the LES predictions compared with those without LES, we first present selected results of the latter.

5.1. *Results for flapping foil without LES*

The instantaneous lift $L(t)$ obtained from our model without LES is first compared with analytical result of Theodorsen (1935) in figure 5. The comparison is satisfactory, with small discrepancies at the extremal values likely due to the assumptions in the theory, of linearized motion and foil geometry, and the use of the inflow velocity for wake convection.

Another solution of this problem is Streitlien & Triantafyllou (1995) who use conformal mapping (of a Joukowski foil) and discrete TE shed vortices advected by local flow. Figure 6 shows a comparison of the present method, Streitlien &

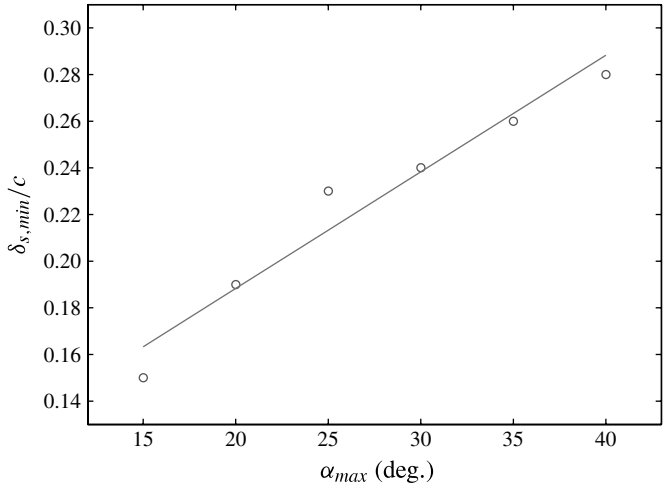

FIGURE 4. Minimum desingularization parameter $\delta_{s,min}$ as a function of α_{max}: results from LES BEM (∘); linear regression given by $\delta_{s,min}/c \approx 0.005\alpha_{max} + 0.09$ (—).

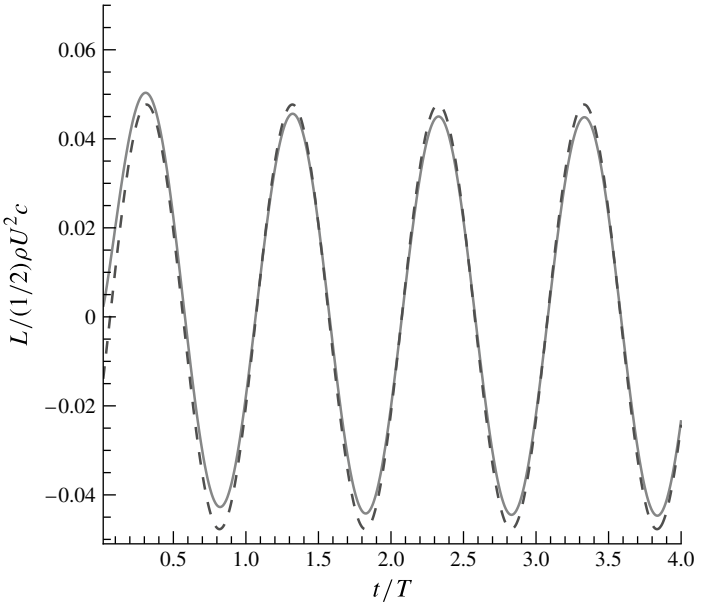

FIGURE 5. Time-dependent lift on a flapping foil without LES: (—) BEM prediction; and (– – –) (linearized) analytical results from Theodorsen (1935). Flapping motion parameters are: $h_0/c = 0.01$, $\theta_0 = 0.01$, $\omega = 1.0$ and $\psi = 0°$.

Triantafyllou (1995), and experimental data from Read *et al.* (2003), for C_T and η. As expected, the BEM and conformal mapping predictions are reasonably close. The notable difference is in η for increasing values of S_t. This is due to the difference in the foil geometries (NACA versus Joukowski) to which η is found to be sensitive for large S_t. The more significant and notable difference in figure 6 is that between

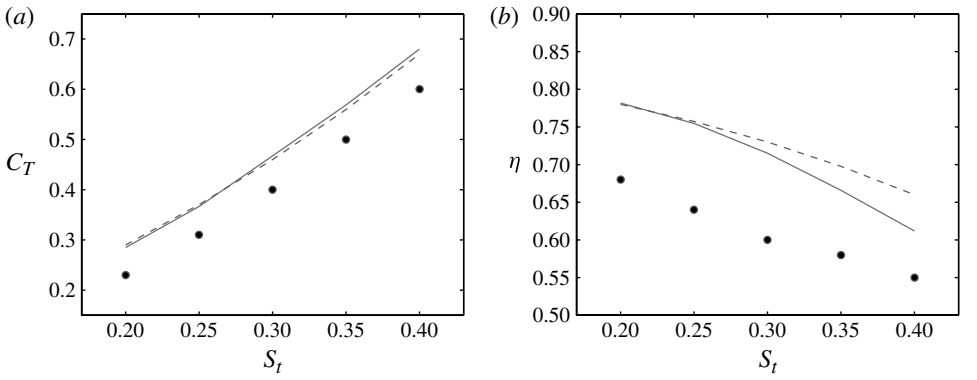

FIGURE 6. Comparison of (*a*) thrust coefficient C_T and (*b*) efficiency η from: (—) BEM without LES; (– – –) numerical results using conformal mapping (Streitlien & Triantafyllou 1995); and (•) experimental measurements (Read *et al.* 2003). Flapping motion parameters are $h_0/c = 0.75$, $\alpha_{max} = 15°$, $\psi = 90°$.

the two numerical predictions (without LES) and the experimental measurements, the former substantially over-predict C_T as well as η over the entire S_t range.

5.2. *Results for flapping foil with LES*

5.2.1. *Vortex structure prediction*

Before showing the force and efficiency predicted by LES BEM, we illustrate the predicted vortex structure and present a comparison with other methods.

The vortex sheets shedding from both trailing and leading edges in a downstroke of the foil are plotted in figure 7. Figure 7(*a*) shows the vortex structure when the foil first heaves to the top position, wherein a vortex sheet shed from the lower side rolls up beneath the foil. The switching criterion comes into effect some time before the foil heaves down to the mean position, figure 7(*b*), which originates a new vortex sheet shed from the upper side. In figure 7(*b*), the earlier shed LE vortex below the foil is shown to be nearly 'attached' along the underside of the foil where evidently the 'fencing' model is now invoked. As the foil heaves down to the bottom of the stroke (figure 7*c*), the near-body vortex configuration resembles that at the top of the stroke in figure 7(*a*). The vortex sheet evolution depicted in figure 7(*a–c*) (with new LE and TE vorticity shed and the entire structure advected downstream) is repeated in each subsequent (half) cycle. The modelling of the vortex evolution with the implementation of desingularization, LES criterion, and the switching and fencing models, resulting in multiple LE vortex sheets over time, is found to be robust and allows simulation over long time.

The configuration and salient features of the predicted vortex sheet evolution can be compared with experimental flow visualization and a Navier–Stokes solution of the problem. Figure 8 compares, for two cases with different motion parameters, the LES BEM results with digital particle image velocimetry (DPIV) images from Anderson *et al.* (1998) and the Navier–Stokes solution from Zhu & Peng (2009) (both for a relatively low Reynolds number of $O(10^{2\sim3})$). The qualitative corroborations among the three are quite satisfactory.

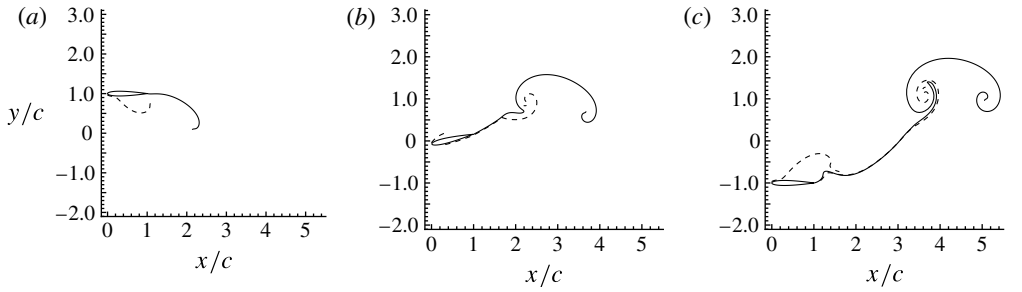

FIGURE 7. Positions of the LE and TE shed vortex sheets $\mathscr{L}(t)$ (– – –) and $\mathscr{T}(t)$ (—) at three instants during the downward stroke of a flapping foil: (a) $(t-t_d)/T=0$; (*b*) $(t-t_d)/T=1/4$; (*c*) $(t-t_d)/T=1/2$. Flapping motion parameters are $S_t=0.3$, $\alpha_{max}=30°$, $h_0/c=1.0$ and $\psi=90°$.

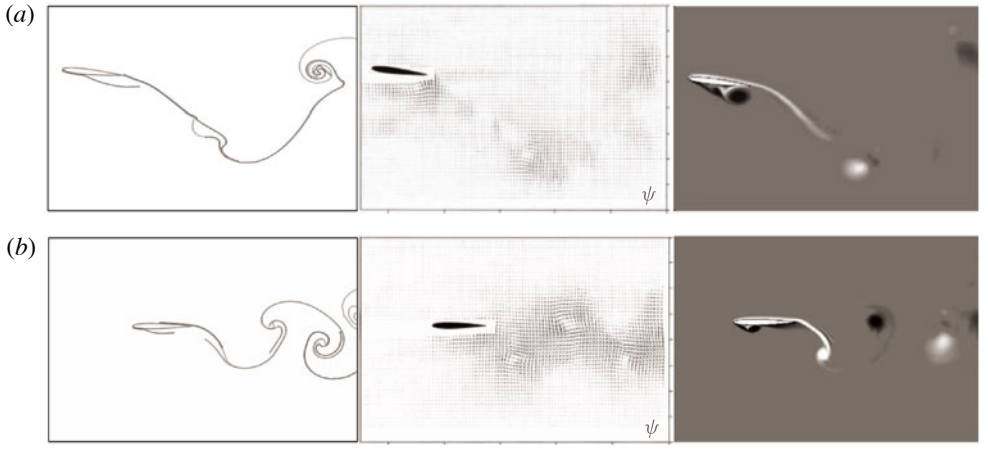

FIGURE 8. Snapshots of LE and TE shed vortex structures from (left) prediction by the LES BEM; (middle) DPIV measurement from Anderson *et al.* (1998); (right) Navier–Stokes simulation from Zhu & Peng (2009), for two cases with (*a*) $S_t=0.36$, $h_0/c=0.75$, $\alpha_{max}=20.4°$, $\psi=75°$ and (*b*) $S_t=0.3$, $h_0/c=0.25$, $\alpha_{max}=28.3°$, $\psi=90°$, when the foil heaves to the top position.

5.2.2. *Performance prediction*

We perform LES BEM simulations for the same geometry and motion parameters for (all) the test cases reported in Read *et al.* (2003). In the experiments, the phase lag between the heave and pitch motion is specified with $\psi=90°$. For harmonic motions with fixed pitch pivot point, the performance coefficients C_T and η are functions only of S_t, α_{max} and h_0/c.

The comparison between experimental measurements and LES BEM numerical predictions for C_T and η is presented for varying S_t and different values of α_{max} in figures 9 and 10 for the two values of heave amplitudes h_0/c considered in Read *et al.* (2003). For the numerical results, we also include for comparison BEM predictions without LES. The performance predictions from LES BEM compares very well with experimental measurements, while those from BEM without LES clearly do not (and, as expected, increasingly poorly with increasing α_{max}). This clearly shows the importance of LES effect in flapping foil performance, which the present numerical

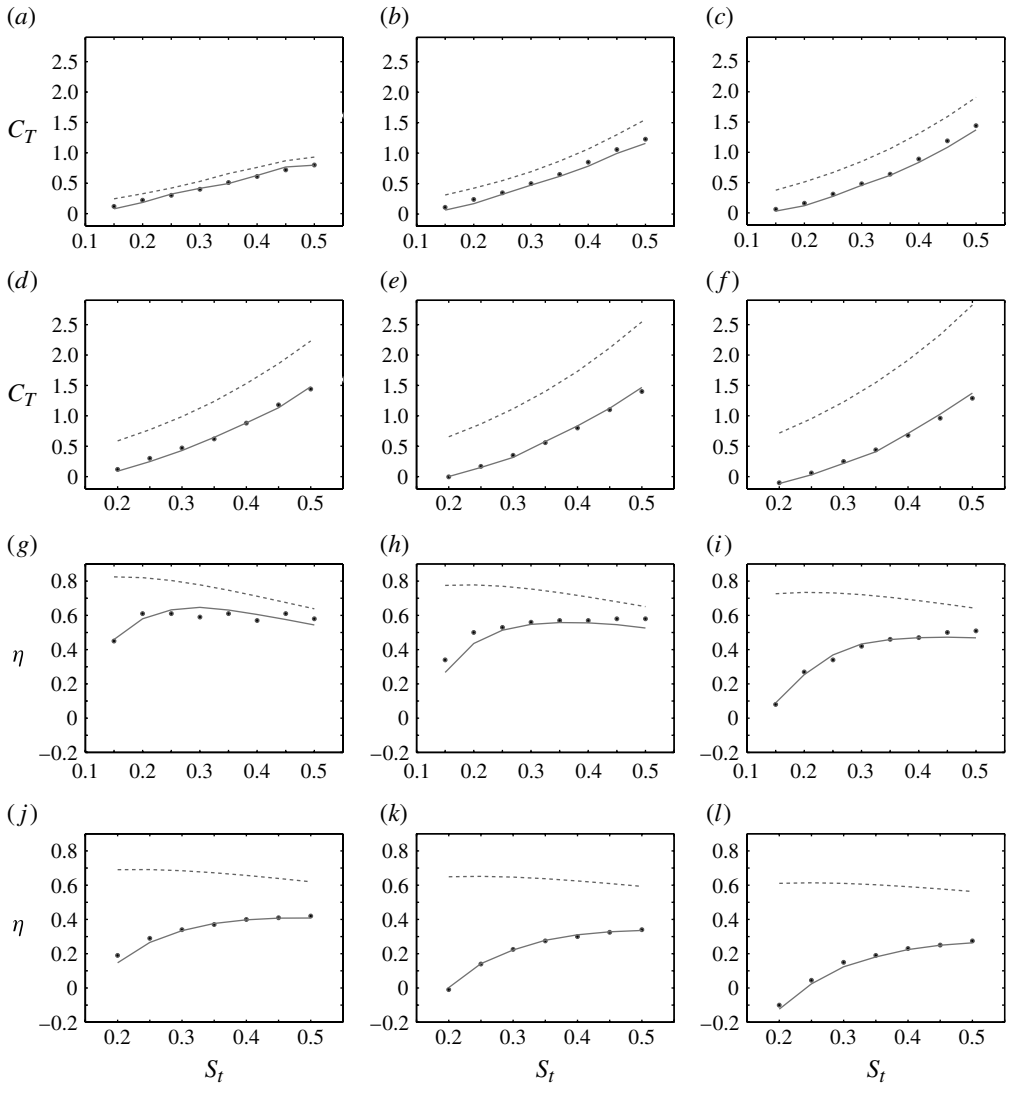

FIGURE 9. Comparison of thrust coefficient C_T (*a–f*) and efficiency η (*g–l*) from (—) LES BEM, (– – –) BEM without LES and (•) experiments of Read *et al.* (2003) at $h_0/c = 1.0$: (*a*) $\alpha_{max} = 15°$; (*b*) $\alpha_{max} = 20°$; (*c*) $\alpha_{max} = 25°$; (*d*) $\alpha_{max} = 30°$; (*e*) $\alpha_{max} = 35°$; (*f*) $\alpha_{max} = 40°$; (*g*) $\alpha_{max} = 15°$; (*h*) $\alpha_{max} = 20°$; (*i*) $\alpha_{max} = 25°$; (*j*) $\alpha_{max} = 30°$; (*k*) $\alpha_{max} = 35°$; (*l*) $\alpha_{max} = 40°$.

approach evidently captures (see figure 8). The excellent quantitative predictions over the broad ranges of S_t and α_{max} is remarkable considering the inherent assumptions and modelling simplifications in the present approach. This also suggests that many physical effects not accounted for here, associated say with viscosity and turbulence, must play a relatively minor role in these cases (the experimental Reynolds number is $O(10^4)$).

Figures 9 and 10 show that the presence of LES in the flapping foil causes both the thrust and efficiency to be lower than would be expected if LES is ignored. For C_T, the difference between these, ΔC_T, generally increases with α_{max} and S_t. For

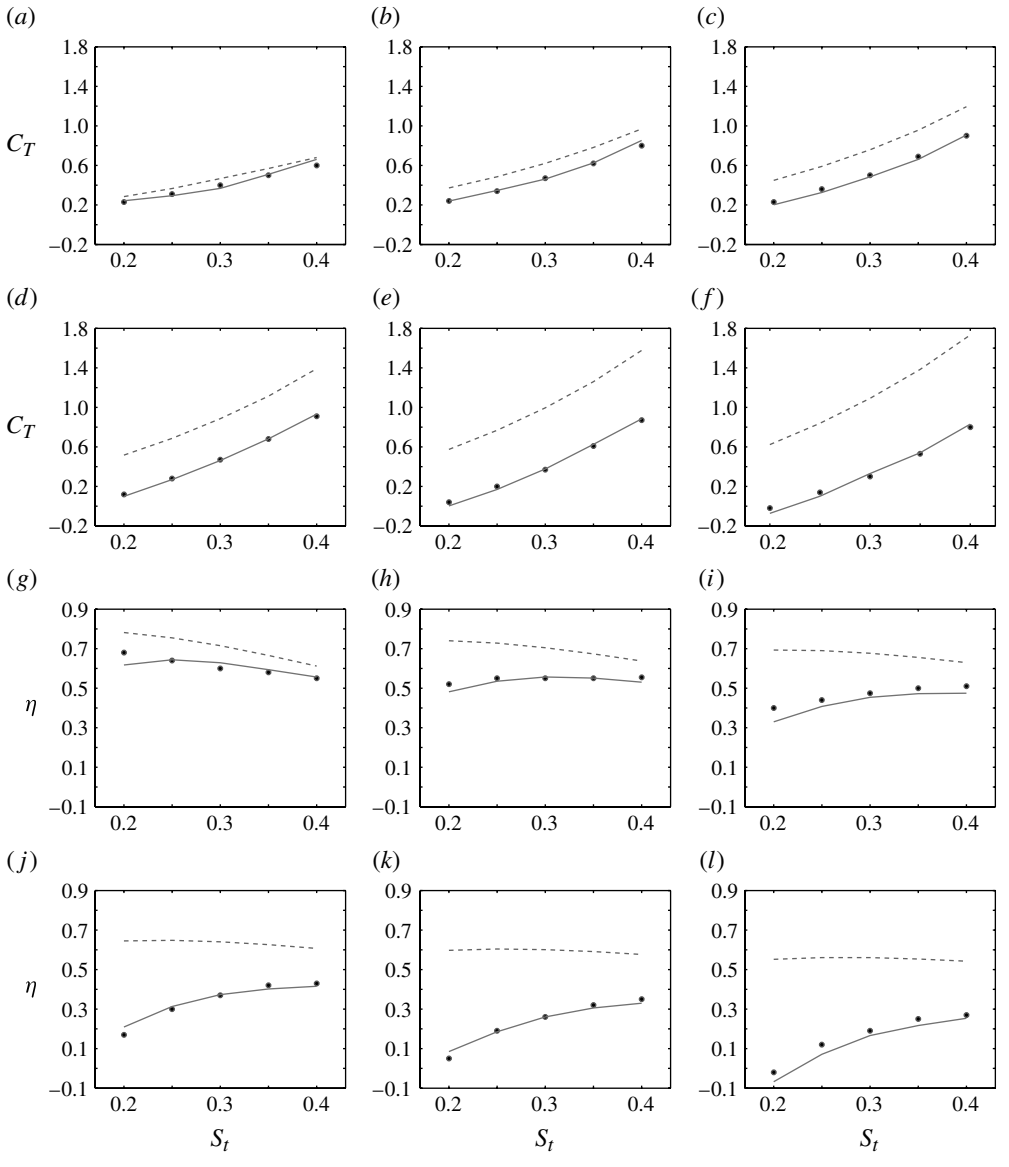

FIGURE 10. Comparison of thrust coefficient C_T (*a–f*) and efficiency η (*g–l*) from (—) LES BEM, (– – –) BEM without LES and (•) experiments of Read *et al.* (2003) at $h_0/c = 0.75$: (*a*) $\alpha_{max} = 15°$; (*b*) $\alpha_{max} = 20°$; (*c*) $\alpha_{max} = 25°$; (*d*) $\alpha_{max} = 30°$; (*e*) $\alpha_{max} = 35°$; (*f*) $\alpha_{max} = 40°$; (*g*) $\alpha_{max} = 15°$; (*h*) $\alpha_{max} = 20°$; (*i*) $\alpha_{max} = 25°$; (*j*) $\alpha_{max} = 30°$; (*k*) $\alpha_{max} = 35°$; (*l*) $\alpha_{max} = 40°$.

$\eta(=C_T/C_P)$, the difference is however more dramatic for small S_t. This is due mainly to the fact that, for (almost) constant ΔC_T, C_P diminishes with decreasing S_t, and the difference in η predictions is amplified (for C_P not significantly changed by LES, which we find to be the case).

The reduction of C_T relative to BEM prediction without LES, ΔC_T, is of practical interest since many existing theoretical/numerical predictions neglect LES. From figures 9 and 10, we see that generally $\Delta C_T = \Delta C_T(\alpha_{max}, S_t)$, with ΔC_T increasing

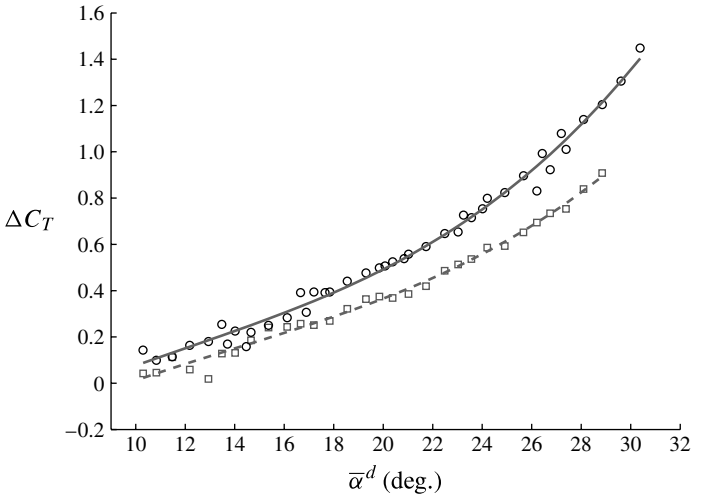

FIGURE 11. Variations of ΔC_T with $\overline{\alpha}^d$: (○) all numerical data from figure 9; (—) fitting curve for all data from figure 9; (□) all numerical data from figure 10; (– – –) fitting curve for all data from figure 10.

monotonically with α_{max} and S_t. Through heuristic reasoning, we find that ΔC_T in, say, the downward stroke can be approximated by $\overline{\alpha}^d$, which is a good measure of the average angle of attack experienced by the foil, and hence the intensity of LES, over this downward stroke. Figure 11 is a plot of $\Delta C_T(\overline{\alpha}^d)$, showing the collapse of all of the data in figures 9 and 10 for the two values of h_0/c.

The thrust reduction ΔC_T can be explained physically in terms of total circulation Γ around the foil. As expected, the presence of LES results in total circulation reduction $\Delta\Gamma$ due to the shedding of LE vorticity opposite to the TE vorticity. The circulation reduction, $\Delta\Gamma$, has a different effect on the quasi-steady T^S and unsteady T^U components of the total thrust T, associated with the quadratic and inertia terms of the Bernoulli pressure (3.2), respectively, $T = T^S + T^U$:

$$T^S \equiv -\frac{1}{2}\rho \int_{\mathscr{B}(t)} (|\nabla\phi(x,y,t)|^2 + 2U\phi_{,x}) n_x \,\mathrm{d}\ell; \quad T^U \equiv -\rho \int_{\mathscr{B}(t)} \frac{\partial\phi(x,y,t)}{\partial t} n_x \,\mathrm{d}\ell. \quad (5.1)$$

In general, the decrease in total circulation, $\Delta\Gamma$, due to LES shedding, results in a decrease in T^S and increase in T^U, respectively the former is due to a decrease in the difference of $|\boldsymbol{U}_\infty + \nabla\phi|^2$ as in the steady problem, and the latter is due to an increase in the difference of ϕ between the upper and lower surfaces of the foil (the picture is qualitatively the same as in the linearized problem; e.g. Katz & Plotkin 1991).

For clarity, we define the unsteady and quasi-steady thrust coefficients C_T^S and C_T^U corresponding to T^S and T^U, respectively. Figure 12 plots C_T^S, C_T^U and $\overline{\Gamma}^u$ $(= -\overline{\Gamma}^d)$ as functions of α_{max}, comparing the results with and without LES. It is seen that the presence of LES significantly reduces $\overline{\Gamma}^u$, which in fact becomes negative, indicating stronger LE shedding than that from the TE. This circulation reduction results in a reduction in C_T^S, accompanied by an increase in C_T^U, consistent with our general analysis above. In general, we find that the reduction in C_T^S is greater than the increase in C_T^U, which leads to the net thrust reduction ΔC_T observed. Reflecting the negative $\overline{\Gamma}^u$, C_T^S is also negative, and the total (positive) thrust is dominated by

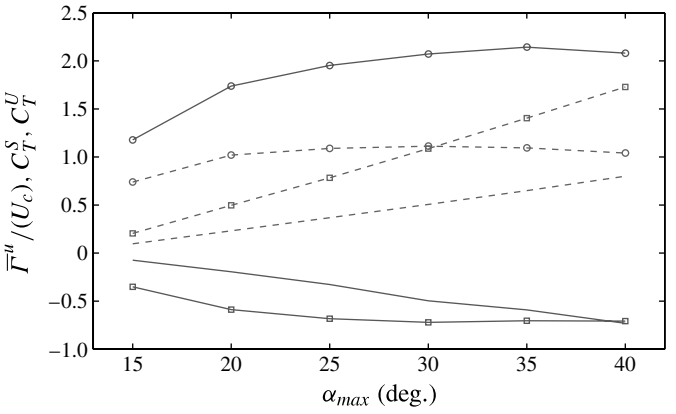

FIGURE 12. $\overline{\Gamma}^u/(Uc)$, C_T^S and C_T^U with varying α_{max}: (—) $\overline{\Gamma}^u/(Uc)$ with LES; (—□—) C_T^S with LES; (—○—) C_T^U with LES; (– – –) $\overline{\Gamma}^u/(Uc)$ without LES; (– □ –) C_T^S without LES; (– ○ –) C_T^U without LES.

unsteady effect from C_T^U when LES is present. In contrast, when LES is neglected, the dynamical picture is qualitatively different, with C_T^S and C_T^U both positive and contributing approximately equally to C_T throughout the α_{max} range. The important role of the unsteady component of the thrust is a distinctive feature of flapping foils with LES.

The significance of LES and the roles of the quasi-steady and unsteady contributions can be seen directly from (5.1). Figure 13 plots the instantaneous distributions of the quasi-steady, p^S, and unsteady, p^U, components of the Bernoulli pressure p on the foil approximately one-third into a downward stroke. The appreciable difference due to LES occurs on the pressure (lower) side of the foil where over most of the surface there is a general elevation of p^U and reduction of p^S (both associated with the overall reduction of $\overline{\Gamma}^u$), and the net contribution of the former to C_T is somewhat mitigated by the latter. Both p^S and p^U experience a significant reduction near a certain point (marked 'A' in the figure), which we find is due to the presence of strong vorticity in the shed $\mathscr{L}$ near that point (see the inset). The net effect of p^S and p^U is shown in figure 13(c) with a uniformly reduced total pressure along the pressure (lower) side and a concentrated low pressure valley, resulting in a reduction of C_T.

6. Application of LES BEM to design

The accuracy of LES BEM in predicting overall performance over broad ranges of the motion parameters, coupled with the robustness and efficiency of the method makes it a useful tool for (preliminary) design of flapping foil motion (and geometry).

To illustrate this, we consider an example problem involving the introduction of higher harmonics into the flapping motion. The addition of higher motion harmonics to improve the performance of flapping foils is suggested by Read *et al.* (2003) who obtained increased average thrust by adding third-harmonic components to the heave motion. For specificity, we consider the problem of maximizing the efficiency of a NACA0012 foil that produces a specified thrust $C_T = C_T^*$ by designing the flapping motion parameters with (versus without) third-harmonic components (clearly odd harmonics are of greater interest on top of the original vertically antisymmetric

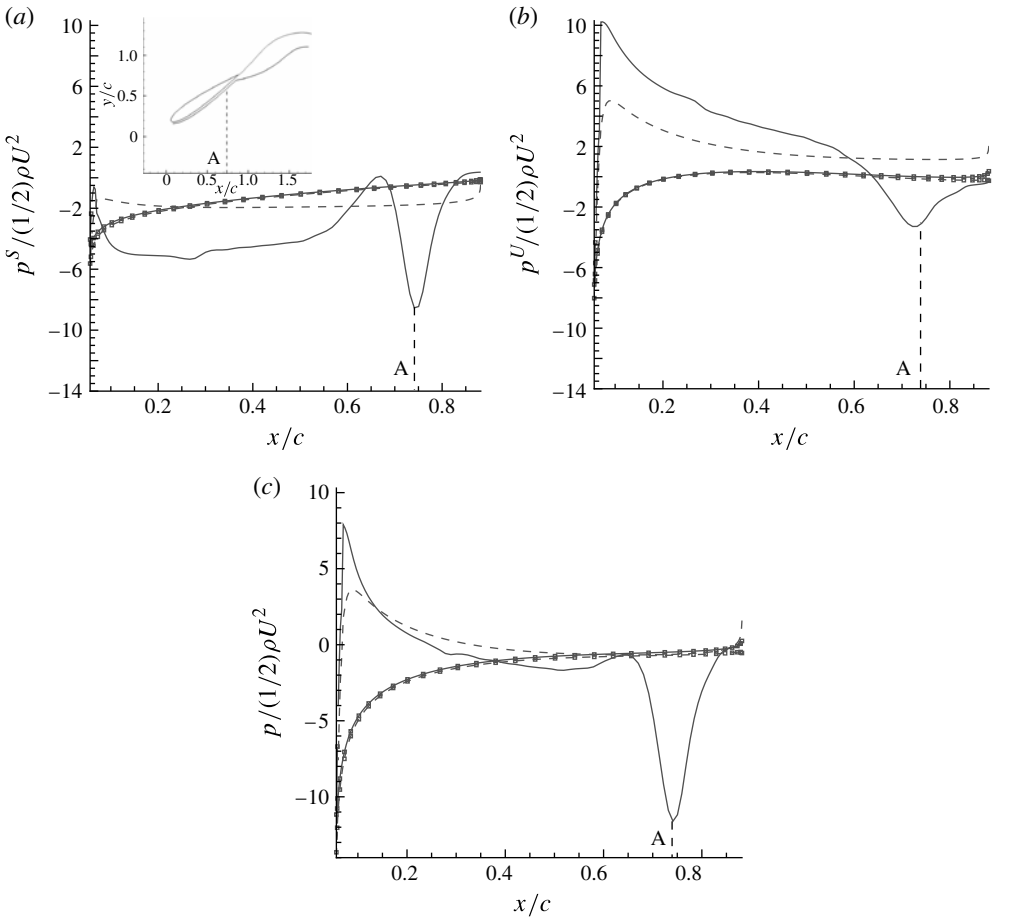

FIGURE 13. Distributions of steady part p^S (*a*) and unsteady part p^U (*b*) of Bernoulli pressure p (*c*) on foil surface approximately one-third into a downstroke: (– – –) pressure (lower) side without LES; (—) pressure (lower) side with LES; (– ⊟ –) suction (upper) side without LES; (—⊟—) suction (upper) side with LES . The low-pressure valley is marked by 'A'. Inset: Instantaneous positions of flapping foil and vortex sheets. The close proximity of the shed vortex sheet and the (lower) foil surface is associated with the fencing model. The motion parameters are $h_0/c = 1$, $S_t = 0.5$ and $\alpha_{max} = 20°$.

flapping problem) in the heave:

$$h(t) = h_0 \sin(\omega t) + h_3(t), \quad h_3(t) = \lambda \sin(3\omega t + \beta), \tag{6.1}$$

where λ and β are amplitude and phase of the third-harmonic component to be determined. For simplicity, we fix $h_0/c = 1$, $\psi = 90°$, so that $\eta = \eta(S_t, \alpha_{max}, \lambda/h_0, \beta)$, and constrain the variable parameters over practically realistic ranges: $0.2 < St < 0.5$, $\alpha_{max} < 40°$, $0 < \lambda/h_0 < 0.1$ and $-10° < \beta < 10°$. The objective is to obtain the optimal efficiency η_{max}, varying the four free parameters S_t, α_{max}, λ/h_0 and β, for different specified values C_T^*. For comparison, we also solve the design problem without h_3. This constrained nonlinear optimization problem is solved using database interpolation and a penalty method (see e.g, Mishima 1996; Luenberger & Ye 2008). With four free

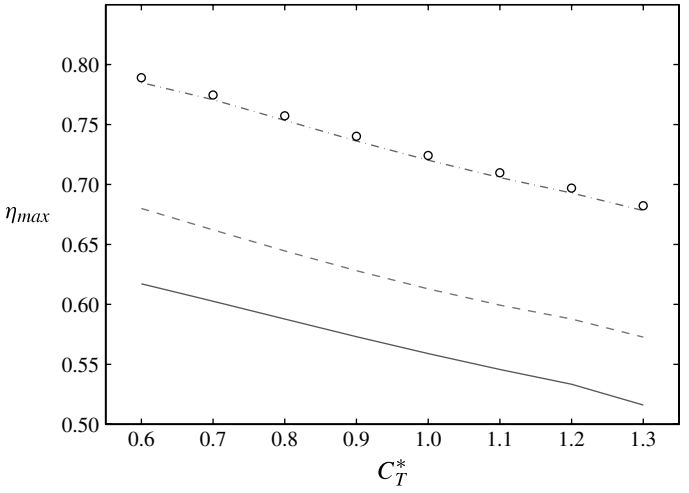

FIGURE 14. Maximum efficiency η_{max} at a range of C_T^*: (—) LES BEM, without h_3; (– – –) LES BEM, with optimized h_3; (– · –) BEM without LES, without h_3; (○) BEM without LES, with optimized h_3.

parameters, the number of evaluations (simulations) involved is large, $\sim O(10^{3\sim4})$, but manageable using LES BEM.

The maximum efficiency η_{max} achieved after optimization is shown in figure 14 (the corresponding optimized motion parameters are not shown) for a range of C_T^*. The maximum efficiency with h_3 is appreciably higher than that without h_3 across the C_T^* range, with $\eta_{max} \gtrsim 60\,\%$ for C_T^* up to $\sim$1.1 (for this case with fixed h_0/c, ψ, and bounds on S_t and β). We also include in figure 14 the corresponding optimization results using BEM without LES. In the absence of LES, the addition of higher-harmonic motions yields no benefit, in fact, $\lambda \approx 0$ for optimal efficiency for the full range of C_T^* we consider.

The difference in the effects of h_3 with and without LES suggests that the improvement of flapping foil performance with h_3 is due to its effect on LES. Analysis of our simulation results with LES shows that the inclusion of (optimal) h_3 relative to the problem without h_3 (but with other motion parameters the same) results in an increase of C_T (and η). Figure 15 shows instantaneous pressure distributions on the foil approximately one-third into a downward stroke, comparing the case with optimized h_3 and with $h_3 = 0$. With the addition of optimal h_3 motion, the low-pressure valley at 'A' seen here and earlier in the lower side pressure distribution when h_3 is not used (cf. figure 13) is almost completely removed. The detailed mechanism obtainable from LES BEM is somewhat involved but the resultant effects on $\mathscr{L}$ is clearly seen in the simulations: qualitatively, the introduction of optimal h_3 results in a weaker and smoother LE vorticity shedding and distribution along $\mathscr{L}$, effectively removing the $\mathscr{L}$-induced low-pressure valley on the pressure side.

7. Conclusions

We develop a numerical method based on a BEM to predict the performance of flapping foil under general motion conditions where LES may occur. The vorticity shed from the LE and TE are treated similarly using desingularized thin vortex sheets,

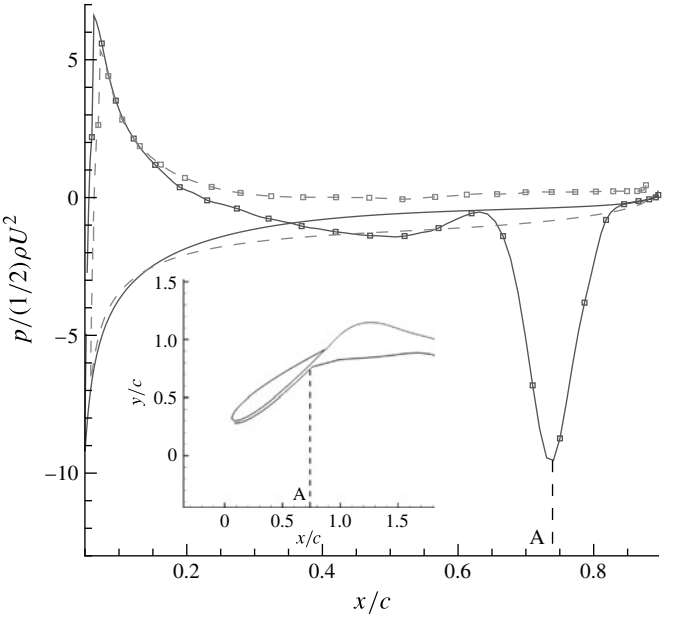

FIGURE 15. Pressure distributions on foil surface approximately one-third into a downstroke: (−⊟−) pressure (lower) side with $h_3 = 0$; (−⊟−) pressure (lower) side with optimized h_3; (—) suction (upper) side with $h_3 = 0$; (– – –) suction (upper) side with optimized h_3. Inset: instantaneous positions of flapping foil and vortex sheets in the presence of h_3. The low-pressure valley is marked by 'A' in the figures. The motion parameters are $S_t = 0.46$, $\alpha_{max} = 18.86°$, with optimized $\lambda = 0.0663$, $\beta = 9.77°$.

with the LE vorticity emanating from a single point determined by a simple criteria based on the location of the LE suction peak. The method is developed for 2D, although the extension to 3D is, in principle, direct.

The prediction of the LES BEM method and experimental measurements of the average thrust and efficiency of the flapping foil compare quantitatively well over broad ranges of motion parameters, in sharp contrast to predictions without LES. This is remarkable considering the theoretical assumptions and modelling simplifications inherent in the present approach. Comparison of the method with and without LES shows that the latter substantially over-predicts the performance of the foil. In the presence of LES, the total circulation is considerably reduced and, under large flapping motions, changes sign. The thrust generation of flapping foil with LES is thus substantially dominated by unsteady effects.

The efficacy of the LES BEM method in predicting flapping performance and its computational robustness and efficiency make it useful for designing the motion and geometry of flapping foils. We illustrate this with an example application of finding the optimal motion parameters including third-harmonic components, say, to maximize efficiency for a specified thrust. The efficiency achieved with optimized third-harmonic motion is appreciably higher than that where only the fundamental harmonic is used. This performance improvement is found to be directly a result of LES wherein the presence of optimized third-harmonic motion is shown to eliminate the vortex-induced low-pressure valley on the pressure side of the foil.

Acknowledgements

We thank Professor M. S. Triantafyllou, MIT, for introducing us to the remarkable performance of the flapping foil, and helpful subsequent discussions especially regarding the experimental data. This research is supported financially by grants from the Office of Naval Research.

REFERENCES

ACHARYA, M. & METWALLY, H. M. 1992 Unsteady pressure field and vorticity production over a pitching airfoil. *AIAA J.* **30** (2), 403–411.

ANDERSON, J. M., STREITLIEN, K., BARRETT, D. S. & TRIANTAFYLLOU, M. S. 1998 Oscillating foils of high propulsive efficiency. *J. Fluid Mech.* **360**, 41–72.

BELLAMY-KNIGHTS, P. G., BENSON, M. G., GERRARD, J. H. & GLADWELL, I. 1989 Convergence properties of panel methods. *Comput. Meth. Appl. Mech. Engng* **76** (2), 171–178.

BURNS, J. H. 1988 A 3-D tunnel correction panel method for swept tapered airfoils with separation. Master's thesis, Department of Aeronautics and Astronautics Engineering, Massachusetts Institute of Technology.

DEGANI, A. T., LI, Q. & WALKER, J. D. A. 1996 Unsteady separation from the leading edge of a thin airfoil. *Phys. Fluids* **8**, 704.

HALLER, G. 2004 Exact theory of unsteady separation for two-dimensional flows. *J. Fluid Mech.* **512**, 257–311.

HE, L. 2010 Numerical simulation of unsteady rotor/stator interaction and application to propeller/rudder combination. PhD thesis, Ocean Engineering Group, Department of Civil Engineering, The University of Texas at Austin.

HESS, J. L. 1990 Panel methods in computational fluid dynamics. *Annu. Rev. Fluid Mech.* **22** (1), 255–274.

ISOGAI, K., SHINMOTO, Y. & WATANABE, Y. 1999 Effects of dynamic stall on propulsive efficiency and thrust of flapping airfoil. *AIAA J.* **37** (10), 1145–1151.

JONES, M. A. 2003 The separated flow of an inviscid fluid around a moving flat plate. *J. Fluid Mech.* **496**, 405–441.

JONES, M. A. & SHELLEY, M. J. 2005 Falling cards. *J. Fluid Mech.* **540**, 393–426.

KÁRMÁN, T. & SEARS, W. R. 1938 Airfoil theory for non-uniform motion. *J. Aeronaut. Sci.* **5** (10), 379–390.

KATZ, J. 1981 A discrete vortex method for the non-steady separated flow over an airfoil. *J. Fluid Mech.* **102**, 315–328.

KATZ, J. & PLOTKIN, A. 1991 *Low-Speed Aerodynamics: From Wing Theory to Panel Methods*. McGraw-Hill.

KINNAS, S. A. & HSIN, C.-Y. 1992 Boundary element method for the analysis of the unsteady flow around extreme propeller geometries. *AIAA J.* **30** (3), 688–696.

KIYA, M. & ARIE, M. 1977 A contribution to an inviscid vortex-shedding model for an inclined flat plate in uniform flow. *J. Fluid Mech.* **82** (02), 223–240.

KOOCHESFAHANI, M. 1989 Vortical patterns in the wake of an oscillating airfoil. *AIAA J.* **27** (9), 1200–1205.

KRASNY, R. 1987 Computation of vortex sheet roll-up in the Trefftz plane. *J. Fluid Mech.* **184**, 123–155.

LEWIN, G. C. & HAJ-HARIRI, H. 2003 Modelling thrust generation of a two-dimensional heaving airfoil in a viscous flow. *J. Fluid Mech.* **492**, 339–362.

LICHT, S., HOVER, F. & TRIANTAFYLLOU, M. S. 2004 Design of a flapping foil underwater vehicle. In *International Symposium on Underwater Technology, 2004*, pp. 311–316. IEEE.

LUENBERGER, D. G. & YE, Y. 2008 *Linear and Nonlinear Programming*. Springer.

MASKEW, B. 1993 *USAERO User's Manual*. Analytical Methods, Inc.

MCCROSKEY, WJ 1982 Unsteady airfoils. *Annu. Rev. Fluid Mech.* **14** (1), 285–311.

MISHIMA, S. 1996 Design of cavitating propeller blades in non-uniform flow by numerical optimization. PhD thesis, Department of Ocean Engineering, Massachusetts Institute of Technology.

MORINO, L. & KUO, C. C. 1974 Subsonic potential aerodynamics for complex configurations – a general theory. *AIAA J.* **12**, 191–197.

PEACE, A. J. & RILEY, N. 1983 A viscous vortex pair in ground effect. *J. Fluid Mech.* **129** (1), 409–426.

READ, D. A., HOVER, F. S. & TRIANTAFYLLOU, M. S. 2003 Forces on oscillating foils for propulsion and maneuvering. *J. Fluids Struct.* **17** (1), 163–183.

REYNOLDS, W. C. & CARR, L. W. 1985 Review of unsteady, driven, separated flows. *AIAA paper*.

ROBINSON, D. E. 1988 Implementation of a separated flow panel method for wall effects on finite swept wings. Master's thesis, Department of Aeronautics and Astronautics Engineering, Massachusetts Institute of Technology.

SARPKAYA, T. 1975 An inviscid model of two-dimensional vortex shedding for transient and asymptotically steady separated flow over an inclined plate. *J. Fluid Mech.* **68** (01), 109–128.

SARPKAYA, T. & SHOAFF, R. L. 1979 An inviscid model of two dimensional vortex shedding for transient and asymptotically steady separated flow over a cylinder. In *17th American Institute of Aeronautics and Astronautics, Aerospace Sciences Meeting*, New Orleans, LA.

SATYANARAYANA, B. & DAVIS, S. 1978 Experimental studies of unsteady trailing-edge conditions. *AIAA J.* **16**, 125–129.

SHUKLA, R. K. & ELDREDGE, J. D. 2007 An inviscid model for vortex shedding from a deforming body. *Theor. Comput. Fluid Dyn.* **21** (5), 343–368.

STRATFORD, B. S. 1959 The prediction of separation of the turbulent boundary layer. *J. Fluid Mech.* **5** (01), 1–16.

STREITLIEN, K. & TRIANTAFYLLOU, M. S. 1995 Force and moment on a joukowski profile in the presence of point vortices. *AIAA J.* **33** (4), 603–610.

TANEDA, S. 1977 Visual study of unsteady separated flows around bodies. *Prog. Aeronaut. Sci.* **17**, 287–348.

THEODORSEN, T. 1935 *General Theory of Aerodynamic Instability and the Mechanism of Flutter*. National Advisory Committee for Aeronautics.

TRIANTAFYLLOU, M. S. & TRIANTAFYLLOU, G. S. 1995 An efficient swimming machine. *Sci. Am.* **272** (3), 64–71.

VISBAL, M. R. 1991 On the formation and control of the dynamic stall vortex on a pitching airfoil. *AIAA Paper* 91-0006.

WANG, Z. J. 2000 Vortex shedding and frequency selection in flapping flight. *J. Fluid Mech.* **410**, 323–341.

YAO, Z. X. & LIU, D. D. 1998 Vortex dynamics of blade–blade interaction. *AIAA J.* **36** (4).

ZHU, Q. & PENG, Z. 2009 Mode coupling and flow energy harvesting by a flapping foil. *Phys. Fluids* **21**, 033601.

ZHU, Q., WOLFGANG, M. J., YUE, D. K. P. & TRIANTAFYLLOU, M. S. 2002 Three-dimensional flow structures and vorticity control in fish-like swimming. *J. Fluid Mech.* **468**, 1–28.